The 5th International Symposium - Supercritical CO2 Power Cycles
March 28-31, 2016, San Antonio, Texas

Paper Number 075

Diffusion bonding of H230 Ni-superalloy for application in microchannel heat exchangers

Monica Kapoor
ORISE Postdoctoral Researcher
National Energy Technology Laboratory
Albany, OR USA
monica.kapoor@netl.doe.gov

Ömer Doğan
Materials Research Engineer
National Energy Technology Laboratory
Albany, OR USA
omer.dogan@netl.doe.gov

Kyle Rozman
ORISE Postdoctoral Researcher
National Energy Technology Laboratory
Albany, OR USA
kyle.rozman@netl.doe.gov

Jeffrey Hawk
Materials Research Engineer
National Energy Technology Laboratory
Albany, OR USA
jeffrey.hawk@netl.doe.gov

Aaron Wilson
Graduate Student
Oregon State University
Corvallis, OR USA
aaron.wilson@oregonstate.edu

Thomas L'Estrange
Graduate Student
Oregon State University
Corvallis, OR USA
thomas.lestrange@oregonstate.edu

Vinod Narayanan
Professor
University of California
Davis, CA USA
vnarayanan@ucdavis.edu

Abstract

Interest in power generation using supercritical CO_2 (sCO_2) cycle has increased in recent years. The sCO_2 cycles rely heavily on heat recuperation to increase

efficiency. Microchannel heat exchangers are proposed to reduce equipment size and enhance heat transfer between heat source and sCO_2. Microchannel architectures are typically formed by a lamination process wherein channels are formed in layers, which are then stacked and diffusion bonded together. Diffusion bonding of Haynes 230 sheets was investigated by modeling the bonding process to determine the optimal process parameters, fabricating diffusion bonded stacks, and tensile testing of these stacks to assess the effectiveness of the chosen processing parameters. Tensile yield strengths of 76-89 % of the base alloy strength were obtained on diffusion bonded stacks. Scanning electron microscopy analysis on the fracture surfaces indicated ductile failure mode in the diffusion bonded zone.

1. Introduction

Due to the potential for improved efficiencies in power generation, interest in sCO_2 cycles has increased in recent years. The sCO_2 cycles rely heavily on heat recuperation for increased efficiency. Microchannel heat exchangers (μHX) are proposed to reduce equipment size and enhance heat transfer between the high-temperature and low-temperature working fluid in sCO_2 power cycles.

Microchannel architectures are typically formed by a lamination process wherein channels are formed in shims, which are then stacked and joined together. One of the most important requirements in μHX is to maintain appropriate channel tolerance to avoid pressure and temperature drop. Diffusion bonding (DB) is one such joining process which provides excellent dimensional tolerances. DB refers to solid-state bonding of stacks of parent material shims/sheets (referred to as sheet henceforth) under pressure and at 0.5-0.85 T_m.

In particular, this study investigates the diffusion bonding of Ni-based superalloys for use in a sCO_2 μHX. The fluid (sCO_2) temperature and pressure during operation of this heat exchanger are in 650˚C-750˚C and 25MPa – 35MPa range, respectively and its anticipated lifetime is approximately 30 years. Currently, only Ni-base superalloys have the high temperature properties that

make them viable as candidate materials under these conditions. The three candidate materials for this application are Haynes 282 (H282), Haynes 230 (H230) and Inconel 740H.

H282 is a gamma prime strengthened alloy which is designed specifically for improved creep strength, weldability and fabricability [1, 2]. H230 is NiCrWMo solid-solution-strengthened alloy which provides excellent creep resistance and oxidation properties near the operating temperature of this solar receiver [3, 4]. Inconel 740H is a relatively young (but ASME approved) alloy developed specifically for ultra-supercritical steam cycles power generation [5]. It is gamma prime strengthened alloy but with a higher Cr (24.5 wt.%) content for enhanced resistance to high temperature corrosion mechanisms. The availability of Inconel 740H was a constraint with the timeline of this project and hence it was not explored as a candidate material.

H230 and H282 are both being studied as candidate materials but these materials have different strengthening mechanisms and different physical metallurgy considerations while selecting the diffusion bonding parameters as well as post bonding heat treatments. Therefore, this manuscript focuses on addressing the challenges related to diffusion bonding of H230. Diffusion bonding of H282 is being investigated as a separate study by itself. Additionally, there is a marked lack of studies on identifying diffusion bond parameters and linking the effect of those parameters to the observed microstructure and eventually to the mechanical properties, particularly for H230 [6]. Consequently, this study addresses how the diffusion bonding parameters were identified, the various microstructures observed, the tensile testing results and microstructure of the fracture surfaces. Last, the use of a Ni-plating on H230 to form an interlayer and facilitate the DB process was also explored.

2. Experimental Procedures

2.1. *Computational model of diffusion bonding*

A computational model was adapted from the work of Hill and Wallach [7] to identify the appropriate time, temperature and pressure for DB of H230 sheets. H230 is a Ni-based superalloy with 22 Cr, 14 W, 2 Mo, 3 Fe, 5 Co, 0.50 Mn, 0.40 Si, 0.30 Al, 0.10 C, 0.015 B (wt.%) with Ni as balance. This model assumes that surface preparation (before the DB process), such as polishing, produces a series of long parallel ridges. When the two binding surfaces are brought together for bonding, the parallel ridges of each surface will touch tip to tip and result in infinitely long parallel cylinders with an elliptical cross-section. This model outputs the time and the strain needed to close these elliptical voids, quantified as % area bonded, in a direction perpendicular to the longer axis of the voids. Based on this description, it stands to reason that the size of the starting elliptical voids will depend on the surface roughness before the DB process.

The results of the model for DB process of Ni-plated (NP) H230 and non-Ni-plated (non-NP) H230, carried out at 1150˚C, is shown in Fig. 1. 1150˚C is an optimal temperature for H230 to balance diffusion processes to form the bond versus to prevent excessive the grain growth [4]. Fig. 1 shows the effect of time (t) and strain % (ε) on the % of area bonded between the two surfaces as a function of pressure used in the DB process. The balance between area bonded and strain (creep) is critical to achieve a uniform bond and to maintain the dimensional tolerance of the microchannels in the μHX. Fig. 1 shows that to bond > 85 % area between the two surfaces with a strain of 2.5%, DB must be performed at 12.7MPa pressure for 8 hrs. A dotted line in Fig. 1 (a) and (b) marks the identified parameters. Consequently, DB process was carried out with these parameters.

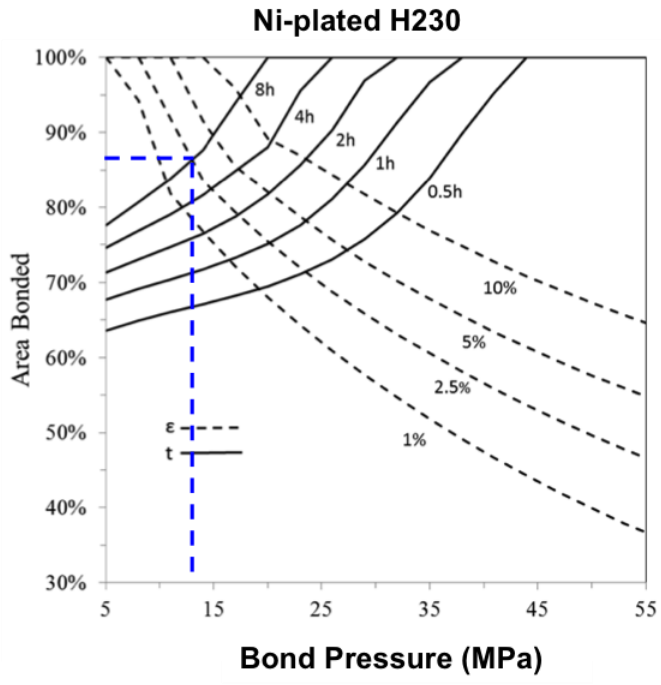

(a)

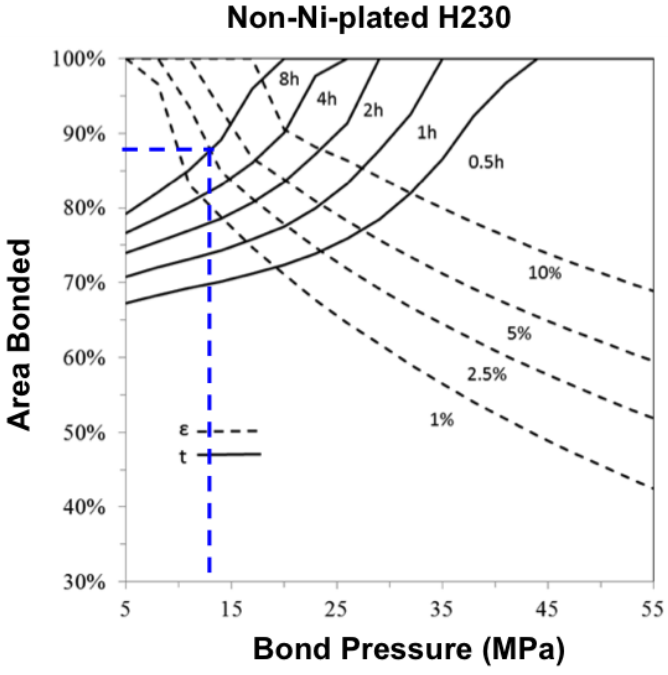

(b)

Fig. 1: Area bonded as a function of pressure during the diffusion bonding process for Ni-plated (NP) H230 and non-Ni-plated (non-NP) H230.

2.2. *Diffusion bonding H230 sheets*

For this preliminary study, the H230 sheets (inset in Fig. 2) with a thickness of ~ 533 μm and 14.5 cm^2 (2.25 in^2) cross-section were DB into stacks containing 100 sheets each, as seen in Fig. 2. Half of these stacks were made with H230 sheet having a 3μm thick Ni-plating (NP) layer to facilitate the bonding process and the other half were made with non-Ni-plated (non-NP) H230 sheet. The surface roughness (Ra) of NP and non-NP H230 sheet is 415 nm and 353 nm respectively. To test the strength of these DB stacks tensile testing specimens were machined out of the stacks such that the loading direction perpendicular to the DB plane, Fig. 2.

Fig. 2: H230 diffusion bonded stack and tensile testing specimens machined from the stack. The inset shows the H230 sheets before they are bonded.

The Ni-plating on the H230 sheets had approximately 12 wt. % P to help lower its melting temperature and bring it closer to the DB temperature of 1150°C. The lower melting temperature of Ni-plating results in a diffusion-brazing-like process with a liquid interlayer at least in the final stages of initial ramping (9 hours from room temperature to 1150°C) of the bonding process. Eventually, diffusion between H230 sheet and the Ni-plating interlayer will alter the composition of the

interlayer and thereby raise its melting temperature. It is likely that by the time the pressure is applied, the interlayer would have solidified [8], as observed in diffusion induced liquid phase bonding of Ni-base superalloy.

2.3. *Microstructure characterization*

Samples measuring approximately 10 mm X 5 mm were cut from the DB stacks for microstructure characterization. These samples contained approximately 5-10 DB regions. The samples were mounted in conductive media and polished to 1μm with a diamond suspension followed by an etch with $CuCl_2$ + HCl + HNO_3 for approximately 15-30 s to delineate the grain boundaries. Scanning electron microscopy (SEM) was performed at 20 KV on FEI Inspect F SEM to quantify the area bonded and the general microstructure of the H230 sheet and the DB region.

Composition analysis to identify a composition gradient across the H230 sheet and DB region is critical because H230 is a solid-solution-strengthened alloy and a composition gradient can alter its strength. Wavelength dispersive spectroscopy (WDS) was performed at 4KV in JEOL 7000 field emission SEM (FESEM) to study the composition profiles across the DB region and the H230 sheets. Low beam energy of 4KV was used to reduce the size of the interaction volume to discern minute differences in composition caused due to diffusion during the DB process. Standards were used to calibrate the microscope before WDS composition analysis. The profiles were obtained from six regions each in NP and non-NP H230.

2.4. *Tensile testing*

Tensile testing was performed at room temperature (RT) and at 750°C, which is close to the operating temperature of these heat exchangers. Tensile tests were performed as specified in ASTM standard E8-13a [9] in an Instron load frame. Solid cylindrical tensile specimens, gauge length of 22.86 mm (0.900 inch) and gauge diameter of 6.35 mm (0.250 inch), were wire electrical discharge machined (EDM) from DB stacks such that the tensile loading was parallel to the stacking

direction, Fig. 2. Contacting extensometers were used to measure the sample strain at RT but the extensometers were removed at 750°C due to slippage and the strain was measured based on the cross head displacement. The samples were preloaded to 0.100 kN and heated, in a clam shell type resistance furnace, at 750°C for 30 minutes to stabilize before load application. Load was applied until failure on an electrically actuated load frame at a constant cross head speed of 0.004 inch/min (0.114 mm/min).

3. Experimental Results & Discussion

3.1. *Microstructure characterization*

To provide a perspective of the macrostructure of DB stack – sheet and the bond – Fig. 3 (a) and (b) show a low magnification optical micrograph of cross section of etched NP H230 DB stack and non-NP H230 DB stack respectively. The DB regions (labeled with arrows) are clearly delineated at a periodicity of approximately 530 μm, which is consistent with the thickness of H230 sheet.

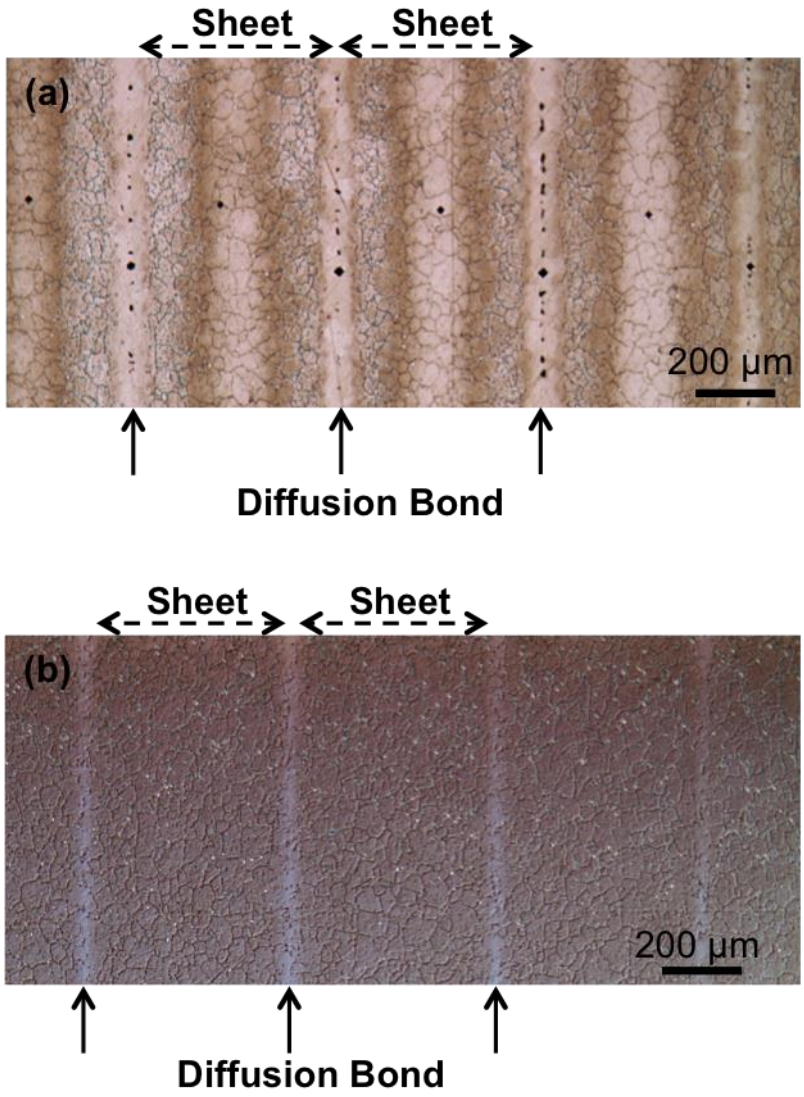

Fig. 3: Optical micrographs of etched (a) Ni-plated and (b) non-Ni-plated H230 DB stack showing the macrostructure of sheet and the diffusion bond in the

One parameter to assess the quality of a diffusion bond is uniformity of microstructure across the bond line. This is often manifested as grain growth across the bond-line, as seen in the close up of the DB regions, Fig. 4 (a) and (b) in both the NP H230 DB stack and non-NP H230 DB stack respectively, indicating a uniform microstructure through the DB. Another parameter to assess accuracy of the computational model used to arrive at the time, temperature and pressure required for the DB process and to assess the quality of the DB is the % area bonded which is quantified using the pores along the bond-line. This % area

bonded is an indication of the void closure between the bonding surfaces during the DB process. The size of the pores in NP H230 DB stack, Fig. 3(a) and Fig.4 (a) is in the 5-10 μm-size range, which seems inconsistent given the initial roughness R_a, 415 nm, of the surfaces before DB. In other words, the size of the pores after DB process is larger than the size of elliptical voids that had to be closed by the DB process. This apparent inconsistency can be explained by the presence of Ni-plating acting as an interlayer, which was partially liquid in the initial stages of the DB process. These large pores can be explained by the liquid movement at the two surfaces due to pressure application during the DB process. No pores were resolved in the non-NP H230 DB stack in an optical microscope.

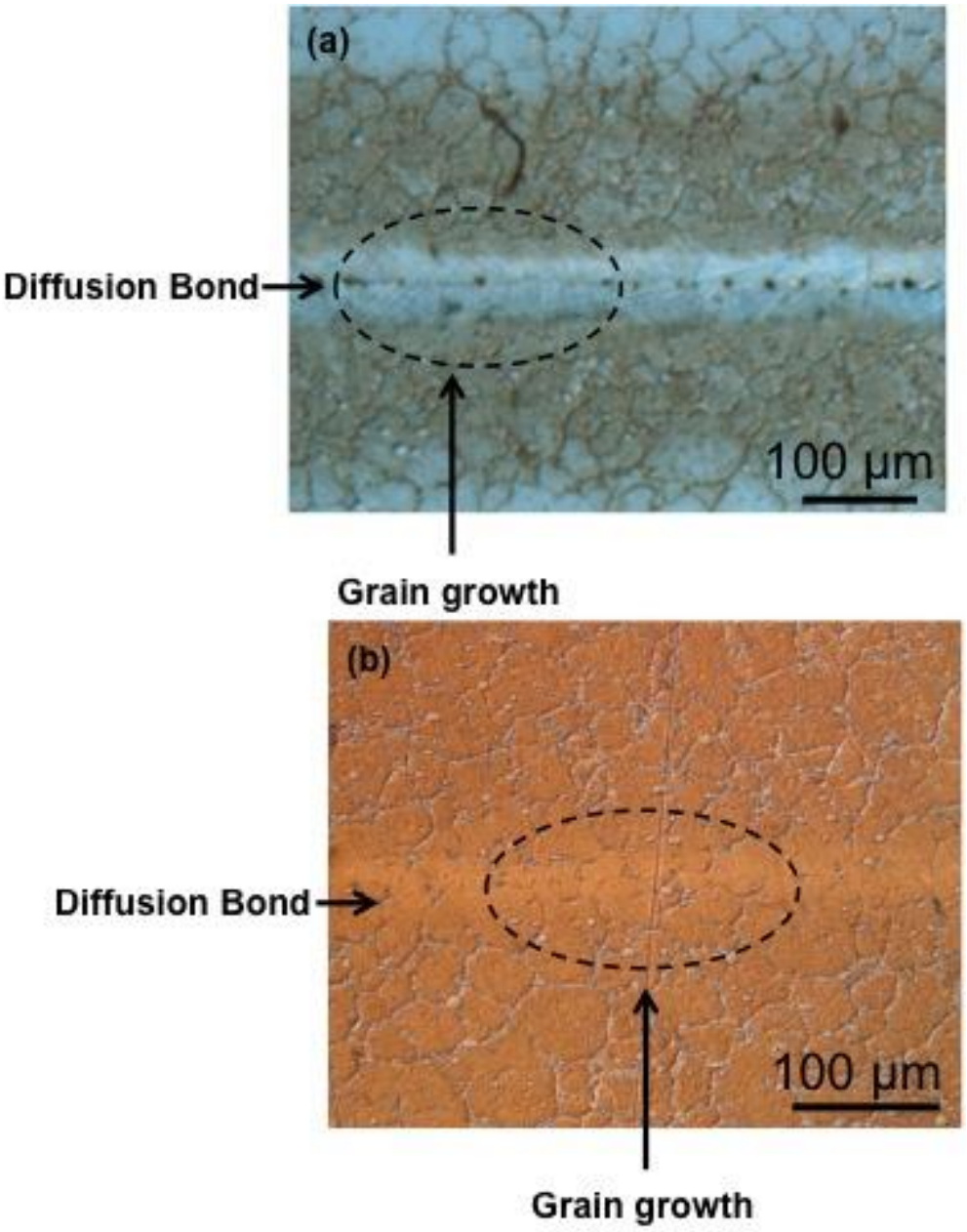

Fig. 4: Optical micrographs of etched (a) Ni-plated and (b) non-Ni-plated H230 DB stack showing the microstructure in the vicinity of the diffusion bond.

SEM was used to observe the microstructure at a higher resolution and specifically check for the presence of pores along the bond line of non-NP H230. Fig. 5 (a) and (b) show the back scattered SEM images of the NP H230 DB stack and non-NP H230 DB stack. Backscattered images show atomic number contrast

and therefore areas containing heavier elements will show up as bright. There are a few observations of note here. First, the pores along the bondline in non-NP H230 DB stack, Fig. 5(b) are smaller (< 1 μm in size) compared to those in NP H230. Fig. 5(a). The size of the pores in non-NP H230 is consistent with the initial roughness R_a, 353 nm, of the joining H230 sheet surfaces. The calculated % area bonded for the NP H230 and non-NP H230 is 10 % and 5.34 % compared to approximately > 10 % predicted by the computational model. The minor differences can be explained by the fact that the model used properties of Ni as some of these properties were not available for H230 superalloy. Additionally, use of Ni-plating resulted in a diffusion-brazing-like process where the interlayer was liquid at least during the initial stages of the bonding. Regardless, the % area bonded predicted by the model and that experimentally calculated values are in close agreement.

Second, the general belief is that the pores would naturally occur along the bond line which should be in a straight line [10]. However, Fig. 5 (b) has quite a few pores which are not along the straight line (labeled with arrows). A close up of the bondline, Fig. 5 (c) shows that the pores which are away from the bondline are along the grain boundaries indicating that these are Kirkendall pores [11]. These pores would be caused due to diffusion from the H230 sheet towards the bondline along grain boundaries. Based on the proximity of these pores to the bond line, it is suggested that this diffusion is concomitant with the grain growth across the bonding surface.

Third, in NP H230 DB stack in Fig. 5(a), the H230 sheet has bright M_6C-type precipitates which are W- and Ni-rich (marked by broken arrows). Additionally, there is an approximately 80μm region which does not have precipitates large enough to be resolved by an SEM. Additional experiments are underway to check for the presence of smaller precipitates in the DB regions.

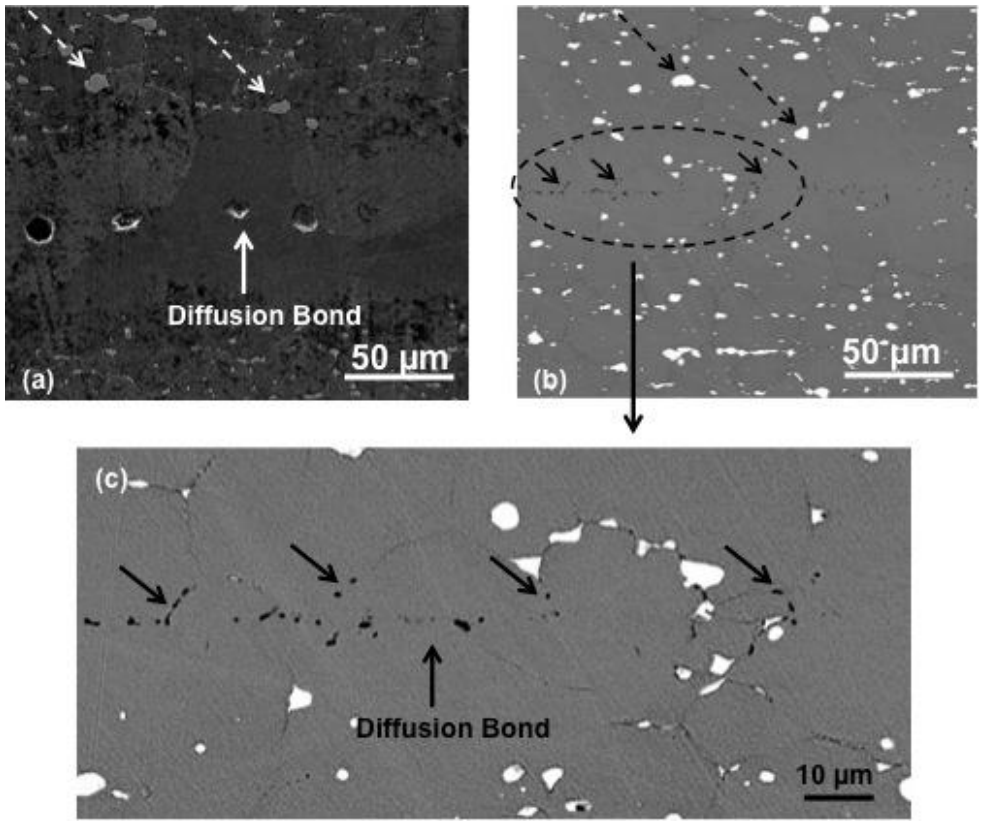

Fig. 5: Backscattered SEM images of (a) Ni-plated and (b) non-Ni-plated H230 DB stack and (c) close up of the bondline in Fig. 5 (b) showing the pores in the vicinity of the diffusion bond.

Since H230 is a solid-solution-strengthened alloy, uniformity of composition across the H230 sheet and the DB region in the DB stack is critical for uniform mechanical properties. Fig. 6 shows a WDS composition profile overlaid on the SEM image to identify the DB region and the H230 sheet from which the profile was obtained. It shows that the composition of Ni, Cr, W, Mo, Co and Fe is uniform between the H230 sheet and DB region.

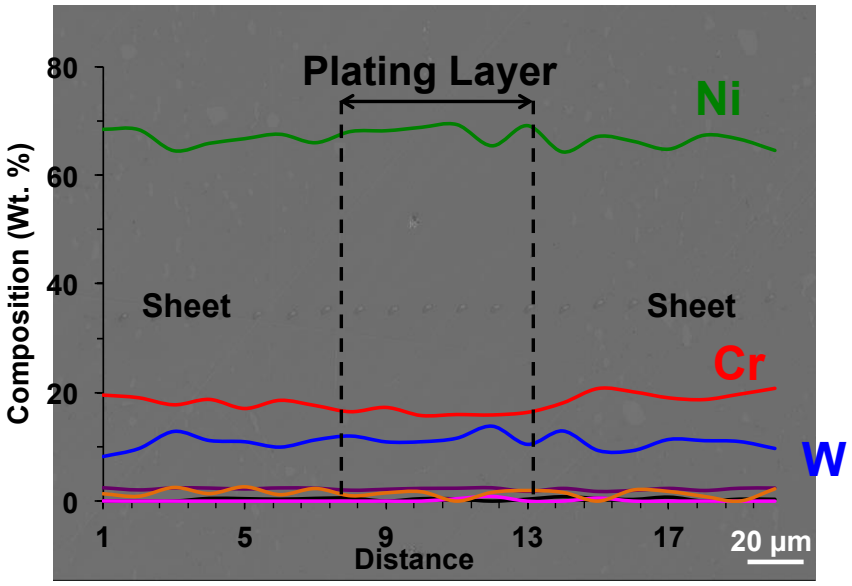

Fig. 6: Composition profile obtained by WDS overlaid on the BSE image of etched Ni-plated H230 DB stack to illustrate the regions through which the profile is obtained. Distance on x-axis the chart is in arbitrary units.

To understand the presence of precipitate-free zones near the DB region in NP-H230 DB stacks, thermodynamic calculations using Thermo-Calc were performed. Haynes international solutionizes H230 at approximately 1250°C which results in the formation of M_6C precipitates (0.026 volume fraction) and leaves approximately 0.03 % C and 11.7 % W (wt. %), the primary precipitate-forming elements, in the matrix. After this step Ni-plating is applied to plates and subsequently the plates are held at 1150°C for 8 h for diffusion bonding process. During this DB process, all elements from the H230 sheet will diffuse into the Ni-plating and equalize the composition, the amount of C in the matrix and the Ni-plating should be less than 0.03 wt. %. Even if it is assumed that 0.03 wt. % C is present in the matrix and the Ni-plating, this C amount is not high enough to form an appreciable precipitate volume fraction, 0.0047, at 1150°C and consequently the precipitates will be too small to be resolved by an SEM. This can help explain the precipitate-free zone observed near the DB region in NP H230 DB stacks.

3.2. *Mechanical Property Testing*

NP H230 and non-NP H230 DB stacks were tensile tested at 750°C and at room temperature (RT) and Fig. 7 presents a summary of the yield strengths of NP DB stack, non-NP DB stack and sheet H230 material. Details of mechanical properties are summarized in Table 1. On testing at 750˚C, the yield strength of non-NP and NP H230 DB stack is 82% and 76 % respectively of the H230 sheet. On testing at RT, yield strengths of non-NP and NP H230 DB stacks were at least 90% of H230 sheet. Regardless of the details, Ni-plating seems to have little effect on the yield strength of the DB H230. However, the difference lies in measured elongation, Table 1.

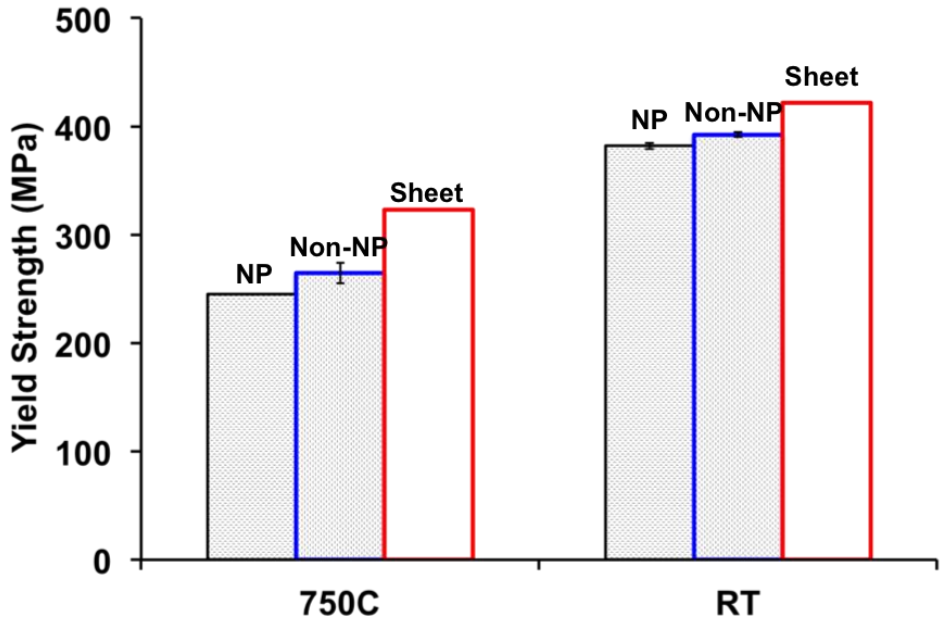

Fig. 7: Yield strength of Ni-plated (NP) and non-Ni-plated (non-NP) H230 DB stacks compared to H230 sheet.

NP H230 DB stacks show an elongation of 1% and 14 % when tested at 750°C and at RT respectively. Non-NP H230 DB stacks show an elongation of 8 % and 22 % when tested at 750°C and at RT respectively. Fig. 8 shows the SEM images of the fracture surfaces and shows that none of the fracture surfaces of DB stacks exhibit any signs of macroscopic ductility. All the samples fractured through

the diffusion bond except non-NP H230 DB stack tested at RT, which fractured through the sheet with the fracture path being multi-planar.

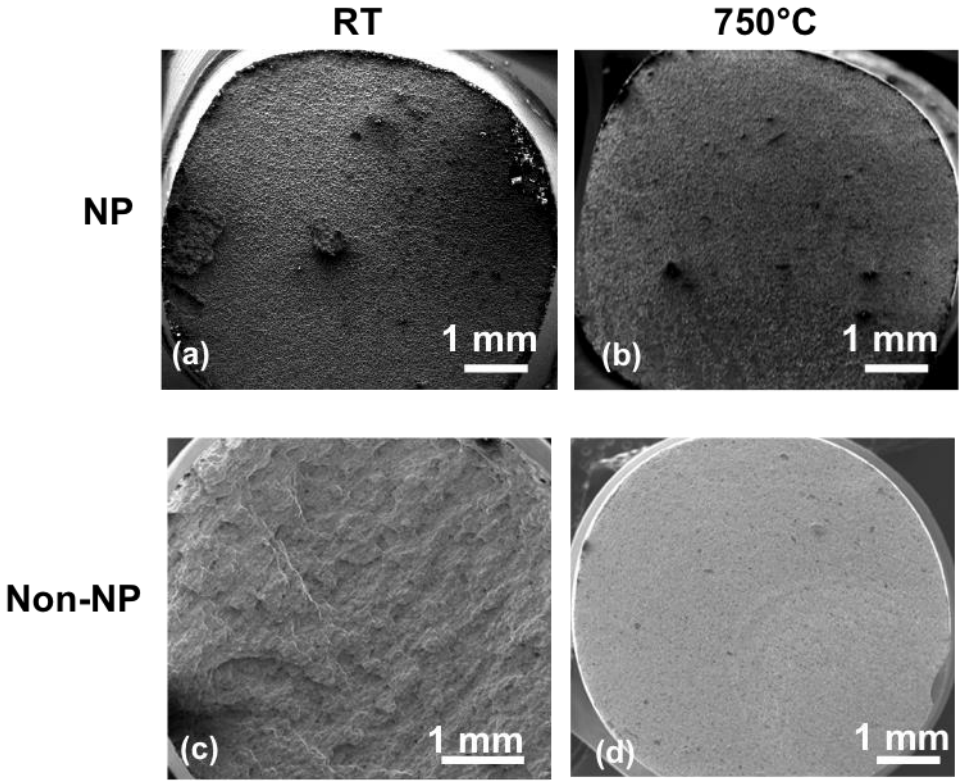

Fig. 8: Fracture surfaces of Ni-plated (NP) and non-Ni-plated (non-NP) H230 DB stacks after tensile testing at room temperature (RT) and at 750°C.

Table 1: Summary of mechanical properties of NP H230, non-NP H230 and H230 sheet (wrought hot rolled) tested at room temperature and at 750°C.

	Yield Strength (MPa)	Ultimate Tensile Strength (MPa)	Ductility Elongation (%)
Room Temperature			
Non-NP DB H230	392	747	21.7
NP DB H230	382	691.5	14.0
H230 sheet	422	838	47.2
750˚C			
Non-NP DB H230	265	379	7.9
NP DB H230	245	281	1.0
H230 sheet	323	539	61.2

A closeup of the fracture surfaces of NP DB stacks, Fig. 9 (a & b), shows that fracture through the DB layer occurs in a typical cup-and-cone manner at the microlevel both at RT and at 750°C. This is despite the limited elongation at the macro level. At RT, Fig. 9(a), the fracture occurs completely through the DB layer but at 750°C, Fig. 9(b), the fracture occurs partially through the H230 sheet. For non-NP DB stacks, the fracture occurs through the H230 sheet at RT, Fig. 9 (c), and through the DB layer at 750°C, Fig. 9 (d).

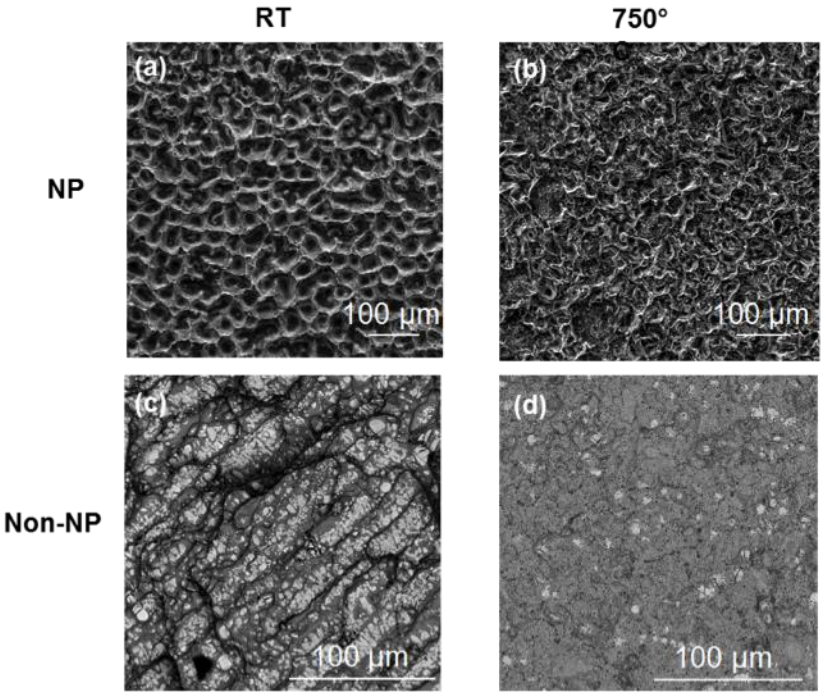

Fig. 9: Fracture surfaces of Ni-plated (NP) and non-Ni-plated (non-NP) H230 DB stacks after tensile testing at room temperature (RT) and at 750°C.

Side view of the non-NP DB stack shows failure occurred in the H230 sheet approximately 250 µm away from the DB, Fig. 10 (a). Microcrack formation (marked with solid arrows) coincides with bands of M_6C carbide precipitates (marked with broken arrows) as seen in Fig. 10 (b). Some of the M_6C carbide precipitates are along the grain boundaries suggesting that subsurface cracking is partially intergranular. Side view of non-NP DB stack tested at 750°C, Fig. 10 (c), shows periodic cracking with the periodicity consistent with the H230 sheet

thickness, i.e. the failure begins at the diffusion bonds. It is suggested that testing at 750°C may provide thermal energy for faster microvoid coalescence which will be exacerbated by the higher density of pores at the bondline resulting in delamination at the bonds.

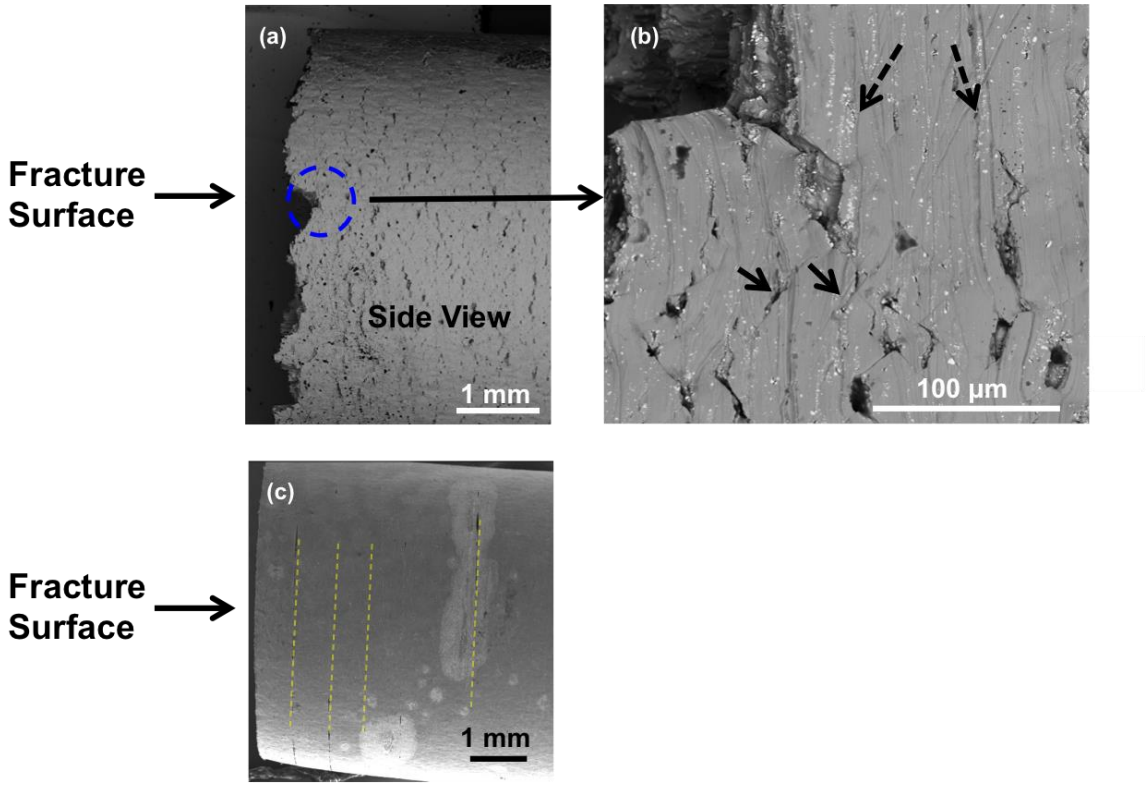

Fig. 10: Side view of the fracture surface of non-NP H230 DB stacks after tensile testing at (a and b) RT and its close up respectively, and (c) at 750°C. The broken arrows point to precipitate bands and the solid arrows point to microcracks.

4. Conclusions

1. The time and % area bonded outputted by the computational modeling of DB of H230 agrees fairly well with the experimentally calculated % area bonded. The experimentally calculated % of voids in NP and non-NP H230 DB stacks is 10% and 5.34 % respectively, which agrees reasonably with the model out put of approximately 10-12 %.

2. In both NP and non-NP H230 DB stacks, a uniform bond with grain growth across the bonds is obtained supported by optical and scanning electron microscopy results.

3. In the NP H230 DB stacks, WDS analysis shows uniform distribution of Ni, Cr, W, Fe, Mo and Co between the sheet and the Ni-plating.

4. Tensile testing of NP and non-NP DB stacks was performed at room temperature and at 750°C. At RT, the yield strength of the NP and non-NP DB stacks is 82.5% and 89% of the sheet material. The failure occurs through the diffusion bond in NP DB stack and through the sheet in non-NP DB stack. At 750°C, the yield strength of the NP and non-NP DB stacks is 76% and 82% of the sheet material. The failure occurs through the diffusion bond in both the cases.

5. The measured elongation is limited concomitant with the absence of classical macroscopic features of a ductile fracture. However, fractography of the surfaces displays features of ductility at the microscopic level.

Acknowledgements

This work was performed in support of the U.S. Department of Energy's Fossil Energy Advanced Combustion Program. The Research was executed through NETL's Research and Innovation Center's Advanced Combustion Field Work Proposal (Richard Dennis and Daniel Driscoll, Technology Managers and Briggs White, Project Monitor). This research was supported in part by an appointment (MK and KR) to the National Energy Technology Laboratory Research Participation Program sponsored by the U.S. Department of Energy and administered by the Oak Ridge Institute for Science and Education. The authors would like to thank Trevor Godell for machining the tensile bars and Christopher Powell for performing the tensile tests.

References

[1] L. Pike. Long Term Thermal Exposure of Haynes 282 Alloy, Superalloy 718 and Derivatives (2010) 644-660.

[2] R.C. Reed, K.A. Green, P. Caron, T.P. Gabb, M.G. Fahrmann, E.S. Huron, S.A. Woodard. Development of a Fabricable Gamma-Prime (γ') Strengthened Superalloy.

[3] L.M. Pike, S.K. Srivastava. Thermal Stability of a Ni-Cr-W-Mo Alloy - Long-Term Exposures, Advanced Materials Research 278 (2011) 327-332.

[4] H.M. Tawancy, D.L. Klarstrom, M.F. Rothman. Development of a New Nickel-Base Superalloy, JOM 36 (1984) 58-62.

[5] J. de Barbadillo, B. Baker, R. Gollihue, S. Patel. Alloy 740H Component Manufacturing Development. Energy Materials 2014. pp. 203-210.

[6] I. Sah, D. Kim, H.J. Lee, C. Jang. The recovery of tensile ductility in diffusion-bonded Ni-base alloys by post-bond heat treatments, Materials & Design 47 (2013) 581-589.

[7] A. Hill, E. Wallach. Modelling solid-state diffusion bonding, Acta Metallurgica 37 (1989) 2425-2437.

[8] N.P. Wikstrom, A.T. Egbewande, O.A. Ojo. High temperature diffusion induced liquid phase joining of a heat resistant alloy, Journal of Alloys and Compounds 460 (2008) 379-385.

[9] ASTM standard E8, 2013 “Standard test methods for tension testing of metallic materials” West Conshohocken, PA: ASTM International.

[10] W.W. Basuki, O. Kraft, J. Aktaa. Optimization of solid-state diffusion bonding of Hastelloy C-22 for micro heat exchanger applications by coupling of experiments and simulations, Materials Science and Engineering: A 538 (2012) 340-348.

[11] D.J. Young. High temperature oxidation and corrosion of metals, Elsevier, 2008.